Electronic Supplementary Material (ESI) for Journal of Materials Chemistry A.

Supplementary Information

A rechargeable Li-CO_2 battery based on preservation of dimethyl sulfoxide

Zhenhua Lu,[a] Min Xiao,[a] Shuanjin Wang,[a] Dongmei Han,[a,b] Zhiheng Huang,[a] Sheng Huang,*[a] Yuezhong Meng,*[a]

[a]The Key Laboratory of Low-carbon Chemistry & Energy Conservation of Guangdong Province, State Key Laboratory of Optoelectronic Materials and Technologies, School of Materials Science and Engineering, Sun Yat-sen University, Guangzhou 510275, China.

[b]School of Chemical Engineering and Technology, Sun Yat-sen University, Zhuhai 519000, China.

*Corresponding Author: mengyzh@mail.sysu.edu.cn
huangsh47@mail.sysu.edu.cn

Experimental Section

CO_2 cathode preparation

Graphene (80%), CNT (10%) and PVDF (10%) were mixed and grinded in NMP to form uniform slurry. The prepared slurry was brushed on Ni Foam by a paintbrush or scraped on carbon paper by a blade, and it was dried in vacuum oven at 60°C for 24 h. After drying, material loaded Ni Foam or carbon paper was punched into 10-mm-diameter circular discs as working electrodes, with 0.10~0.14 mg of active material (the mass of graphene and CNT) on each.

Theoretical Calculations

The solvation structure of Li^+, $TFSI^-$ and different solvents (DMSO, GBL, TEGDME and PC) is investigated by theoretical calculation of atomic configurations and binding energies, which are based on density functional theory (DFT) within the Perdew–Burke–Ernzerhof generalized gradient approximation (GGA-PBE). The double numerical plus polarization (DNP) basis set as well as the DFT semi-core Pseudopots (DSPP) were used. The convergence criterions were set as: energy 1×10^{-5} Ha. Besides, a Fermi smearing of 0.003 Hartree and a global cutoff of 4.4 Å were also used to improve the computational performance. For geometric optimization, the atomic position is fully relaxed until the residual forces on constituent atoms became less than 0.02 eV $Å^{-1}$. The conjugate gradient algorithm was used for ionic relaxation. Herein, the binding energy (ΔE) is defined as:

$$\Delta E = E_{\mathrm{total}} - E_{\mathrm{Li(+)}} - E_{\mathrm{TFSI(-)}} - \mathrm{n}E_{\mathrm{solvent}}$$

Where E_{total} is the total energy of the solvated system, $E_{\mathrm{Li(+)}}$, $E_{\mathrm{TFSI(-)}}$ and E_{solvent} are the energy of the Li^+, $TFSI^-$ and solvent respectively, and n is the number of solvents involved in solvation. The definition indicates that a more negative value depicts a more stable solvated system. Meanwhile, the solvated size was evaluated by using the largest diameter measured of the solvation structure.

Electrochemical Measurements

The 2032-type coin cells without or with holes on the positive side were used for the electrochemical measurements. The cell fabrication was conducted in an Argon filled glovebox. Li metal anode (15.8 mm in diameter) and glass fiber separator (Whatman) were adopted. 1 M LiTFSI (DMSO (or TEGDME, GBL, PC)) and 4 M LiTFSI (DMSO) were used as electrolyte. The cyclic voltammetry (CV) measurements were conducted on an electrochemical workstation with the scan rate were of 0.5 mV s^{-1}. The electrochemical impedance spectroscopy (EIS) was conducted in the frequency range of 10^5 Hz to 0.1 Hz and linear sweep voltammetry (LSV) was conducted at a scan rate of 1 mV s^{-1} in the voltage range of 0 – 5.1 V. The symmetric Li||Li cells with holes and Li-CO_2 battery were tested in a box filled with Ar (0.1 MPa) or CO_2 (0.12 MPa) using a Neware instrument at 28 °C, respectively, and the symmetric Li||Li cells without holes was test by a Land instrument at 28 °C.

Material characterization

The surface morphologies of cycled cathode were imaged by SEM on an TESCAN CLARA scanning electron microscope. The ionic conductivity of the electrolyte was observed with conductivity meter (DDS-11A). The structure of the charge and discharge products were characterized with X-ray powder diffractometer (XRD, Empyrean). The zeta potential was investigated by a zeta potential analyzer (Zetasizer nano 2S). The electrolyte and cycled cathode were characterized by Raman spectra (Renishaw inVia) with 785 nm and 532 nm excitation laser, respectively. The surface composition of cathode and powder sample were characterized by XPS (AXIS SUPERA). ^{7}Li and ^{19}F NMR and self-diffusion coefficient were performed on a Varian Inova 500 MHz NMR.

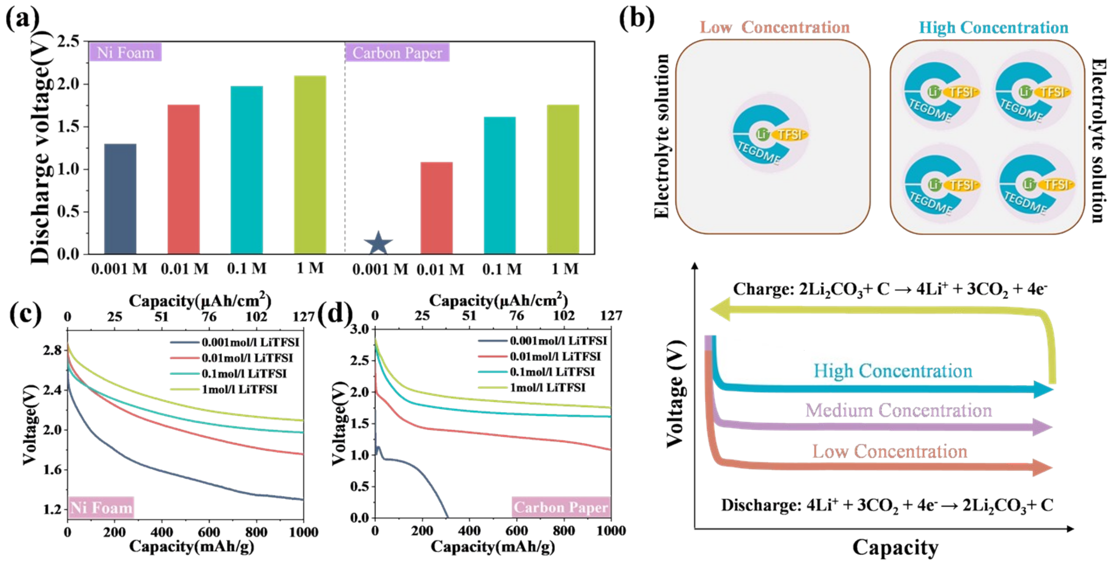

Figure S1. a) The discharge voltage of batteries with different LiTFSI concentration and current collectors (the discharge voltage of Li-CO_2 battery using Ni Foam as current collector for 0.001 M, 0.01 M, 0.1 M, 1 M LiTFSI (TEGDME) electrolyte are 1.29 V, 1.75 V, 1.97 V, 2.09 V, respectively, which is nearly the same for carbon paper, indicating that a higher concentration of Li ion depicts a higher discharge voltage. The value is indicated by an asterisk when discharge voltage is below 0. b) The schematic diagram of different concentrations LiTFSI (TEGDME) and corresponding discharge voltage. The detailed discharge–charge profiles of using different current collectors: c) Ni Foam and d) carbon paper.

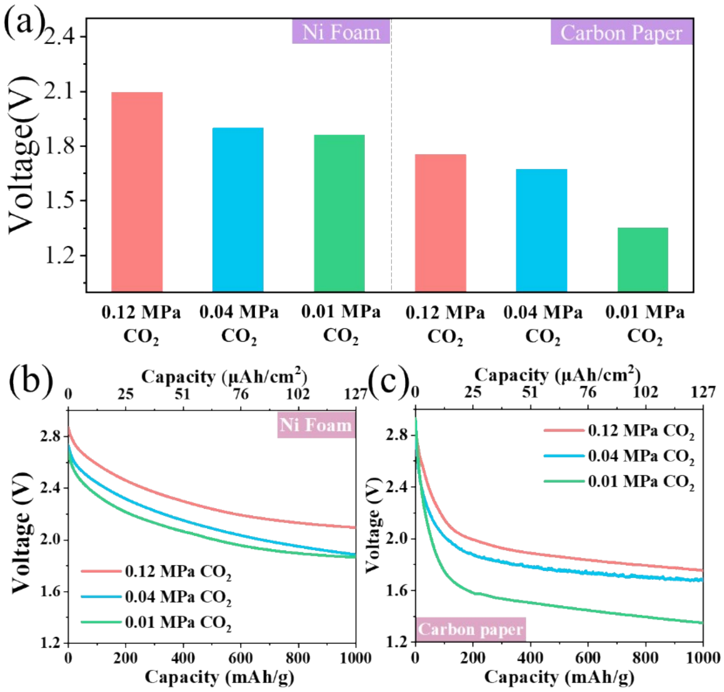

Figure S2. a) The discharge voltages in different pressure of CO_2 using different current collectors. The discharge voltage of Li-CO_2 battery using Ni Foam as current collector for 0.12 MPa, 0.04 MPa, 0.01 MPa (CO_2) are 2.09 V, 2.01 V, 1.88 V respectively, which is nearly the same for carbon paper, indicating that higher concentration of soluble CO_2 depicts a higher discharge voltage). The detailed discharge–charge profiles using different current collectors: b) Ni Foam and c) carbon paper.

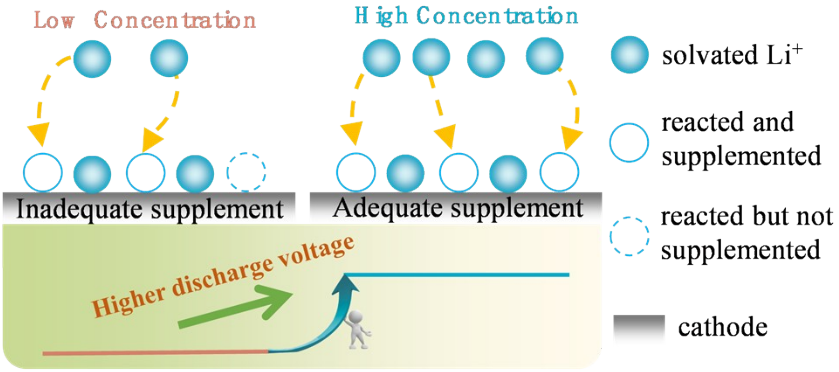

Figure S3. Schematic images of the relationship of concentration and discharge voltage. Nernst Equation describe the effect of concentration in solution on voltage. In fact, the voltage is directly affected by interfacial concentration. However, when the electrochemical reaction starts, the low-concentration reactant in solution cannot supplement to the interface in time, so the interfacial concentration and thus the voltage decrease. In the contrary case of high concentration, the interfacial reactant could be adequately supplemented from the bulk solution. So the voltage remain high during reaction.

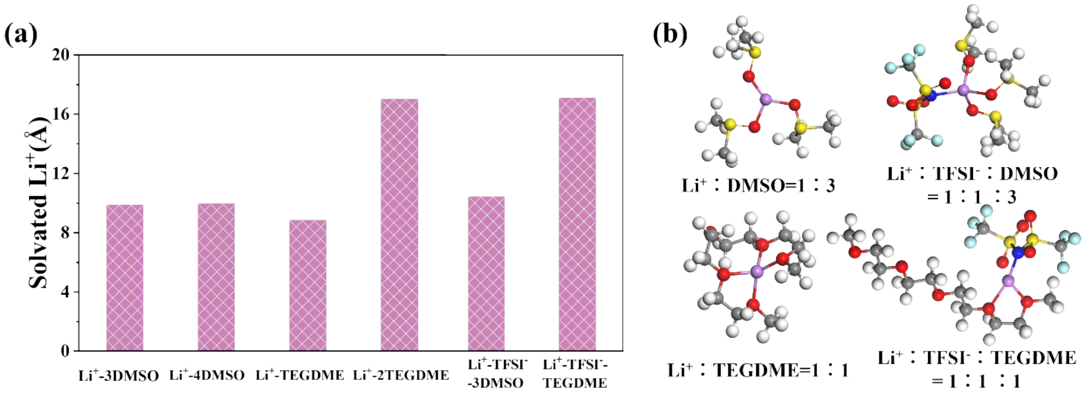

Figure S4. a) Li$^+$ solvated size of Li(DMSO)$_3^+$, Li(DMSO)$_4^+$, Li(TEGDME)$^+$, Li(TEGDME)$_2^+$, Li(DMSO)$_3^+$-TFSI$^-$, Li(TEGDME)$^+$-TFSI$^-$, and the solvated size was evaluated based on the structure. b) The most probably stable solvation structures and corresponding Li$^+$ to solvent and anion ratios of the structures.

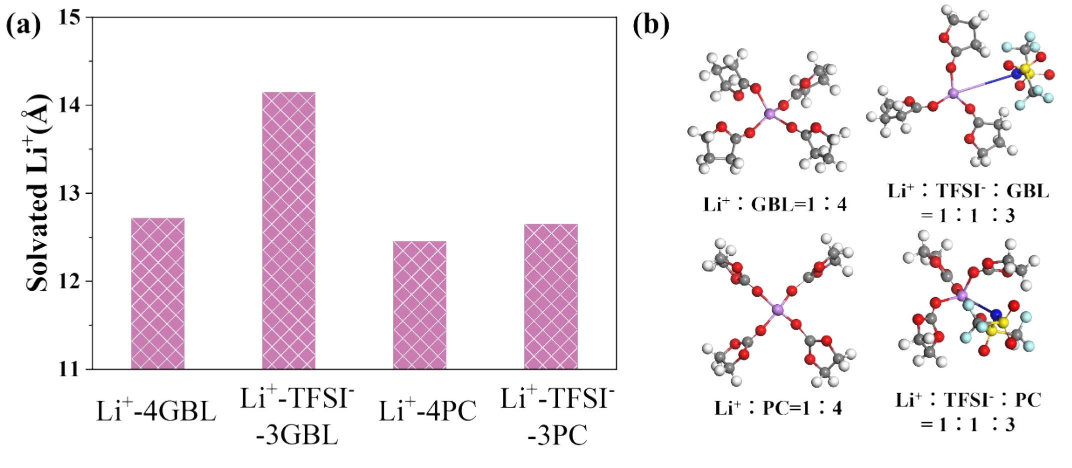

Figure S5. a) Li$^+$ solvated size of Li(GBL)$_4^+$, Li(GBL)$_3^+$-TFSI$^-$, Li(PC)$_4^+$, Li(PC)$_3^+$-TFSI$^-$, and the solvated size was evaluated based on the structure. b) The most probably stable solvation structures and corresponding Li$^+$ to solvent and anion ratios of the structures.

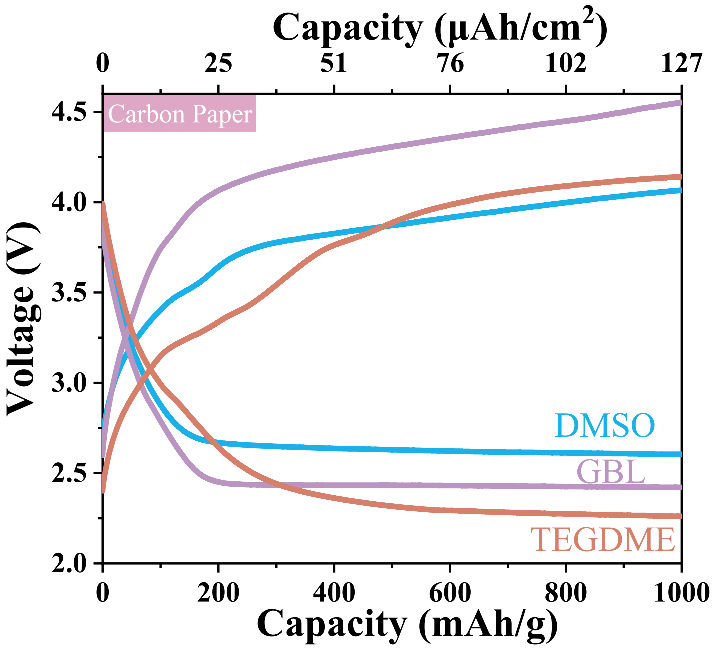

Figure S6. The discharge–charge profiles for the batteries with different electrolyte solvents using carbon paper as current collector with 1 M LiTFSI.

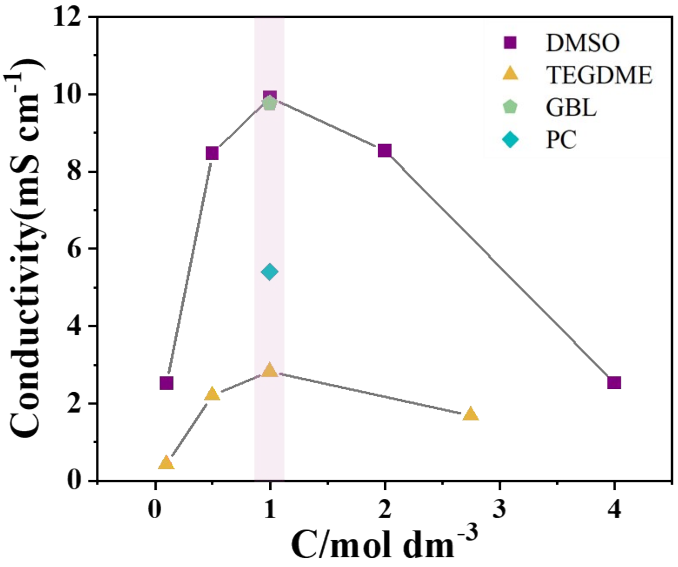

Figure S7. Ionic conductivity of the electrolyte with LiTFSI in different electrolyte solvents and concentrations.

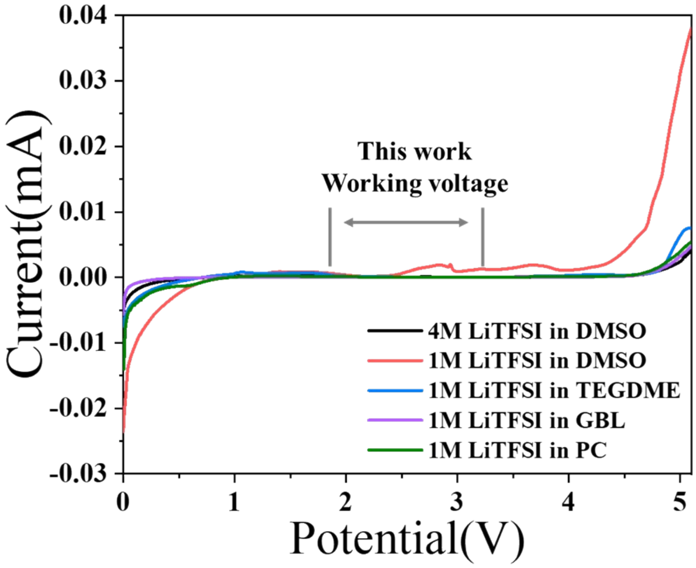

Figure S8. Linear Sweep Voltammetry (LSV) (electrochemical windows) of the carbon paper||Li batteries with different electrolytes. Scan rate: 0.1 mVs^{-1}. Voltage window: 0.0 – 5.1 V versus Li/Li^{+}. The oxidation potential of the battery with 1 M LiTFSI (DMSO) is around 2.5 V, indicating the reaction has occurred between Li anode and free DMSO. And the reaction is stronger when the potential is higher than 4 V. To increase the concentration of LiTFSI to 4 M has alleviated the reaction.

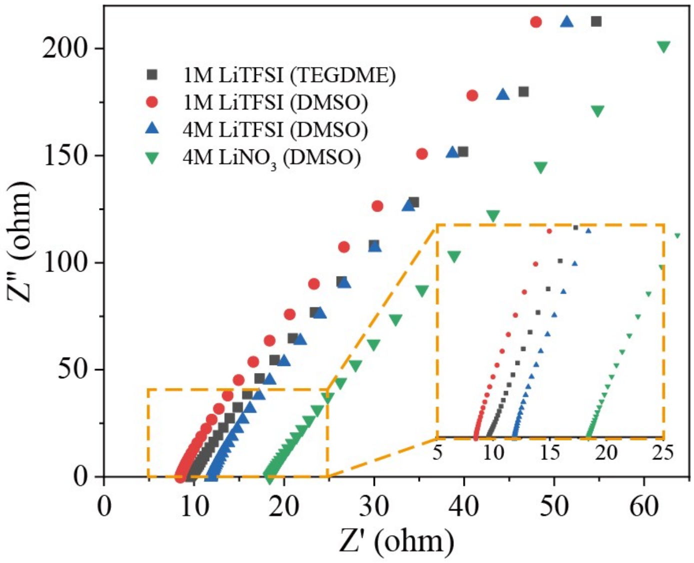

Figure S9. Electrochemical impedance spectra (EIS) of steel symmetrical battery with different electrolytes. The highest impedance of 4 M $LiNO_3$ (DMSO) among those electrolytes derived from the poor dissociation of $LiNO_3$.

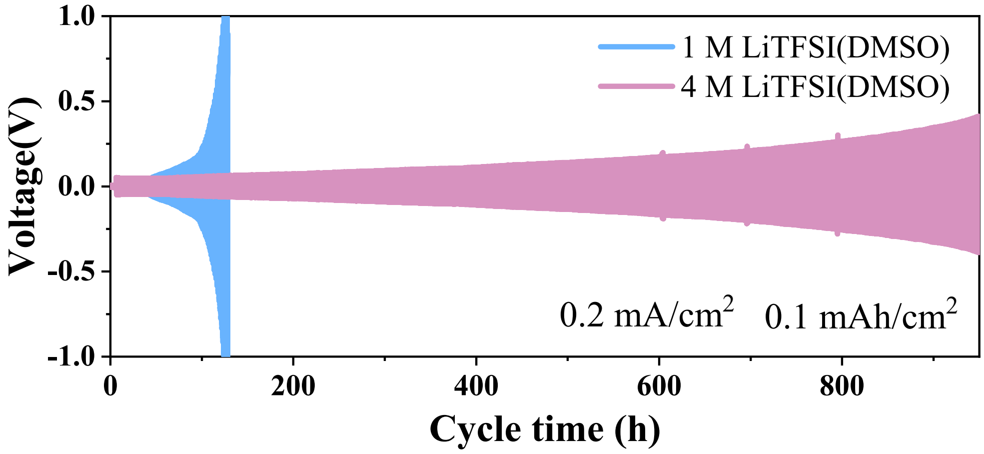

Figure S10. Cycling performance test of Li||Li symmetric battery using 1 M LiTFSI(DMSO) and 4 M LiTFSI(DMSO) as electrolyte at 0.2 mA/cm^2 with a cut-off capacity of 0.1 mAh/cm^2.

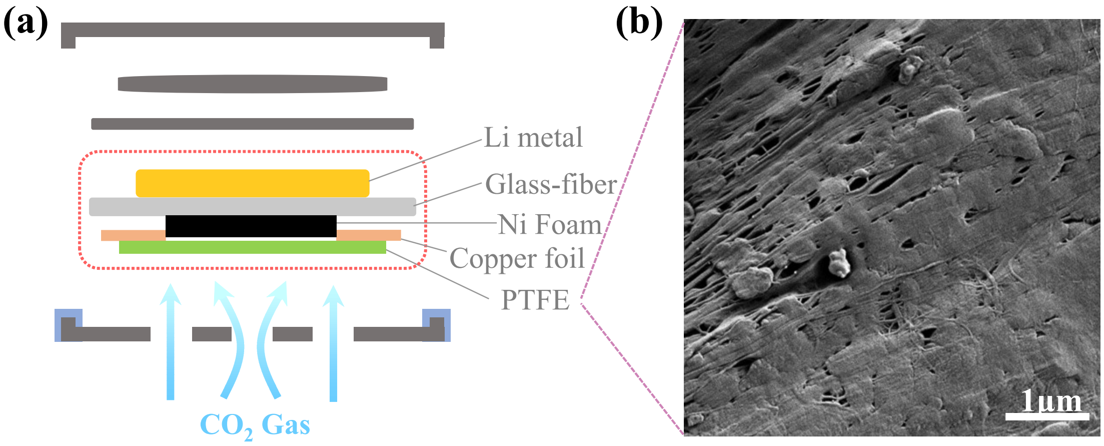

Figure S11. a) The detailed structure of assembled Li-CO$_2$ battery in this work. b) SEM image of PTFE.

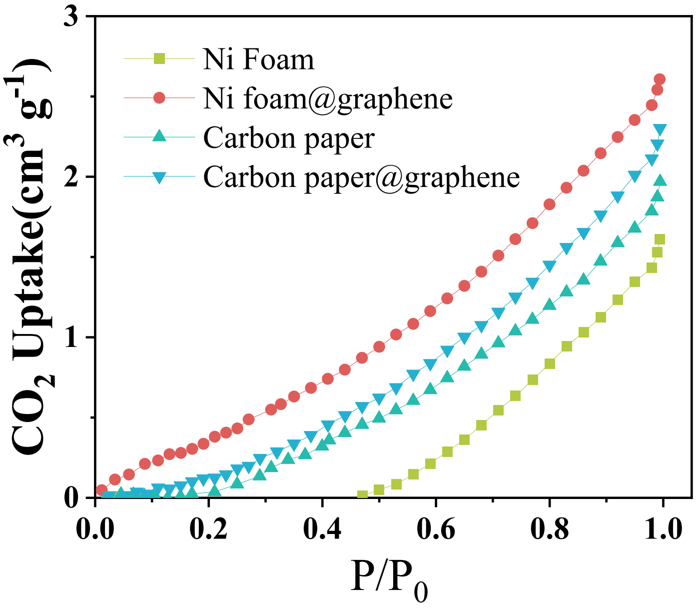

Figure S12. CO$_2$ uptake for Ni foam and carbon paper with or without graphene loaded.

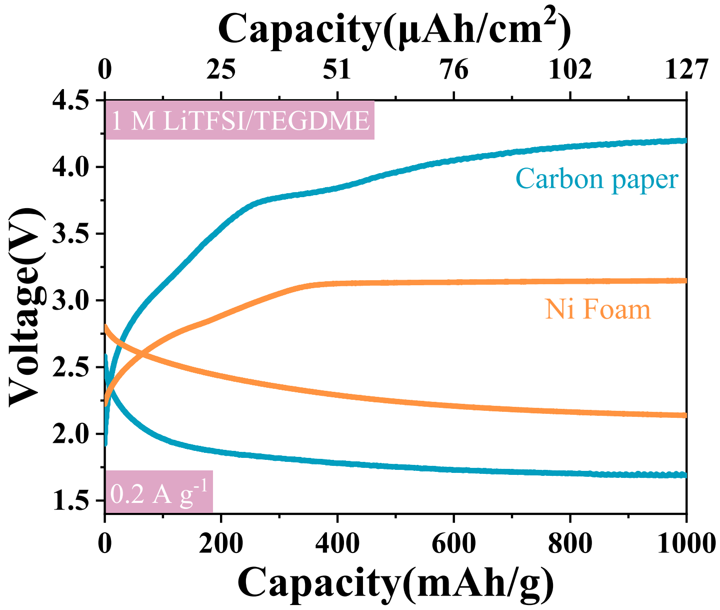

Figure S13. The respective discharge-charge curves of Li-CO$_2$ battery (1 M LiTFSI (TEGDME)) using carbon paper and Ni foam as current collector at 200 mA/g with a limited specific capacity of 1000 mAh/g.

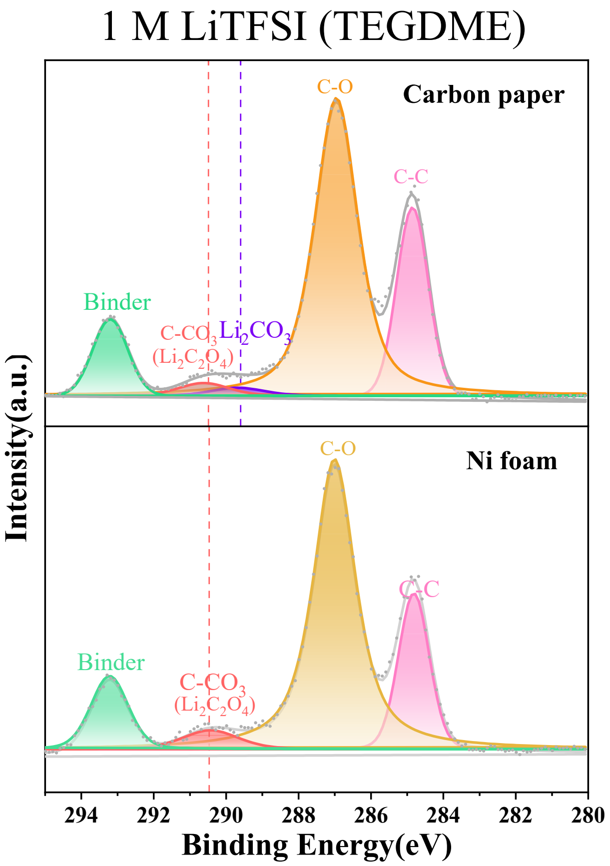

Figure S14. XPS spectra of C 1s regions for discharged cathode after 5 cycles with 1 M LiTFSI (TEGDME) using different current collectors: Carbon paper and Ni foam. $Li_2C_2O_4$ (290.4 eV) also made up the majority in the discharged cathode of Ni-foam based battery after 5 cycles.

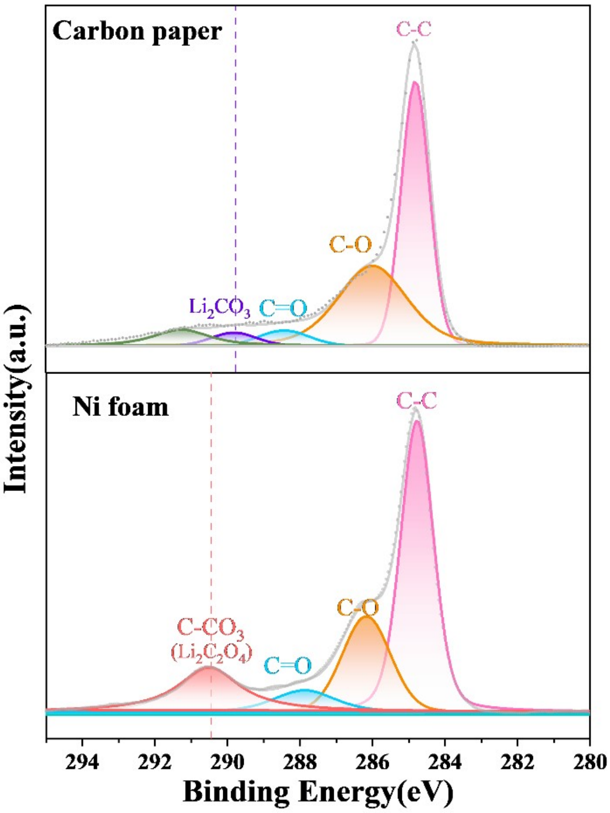

Figure S15. XPS spectra of C 1s regions for vacuum-dried (25°C) Ni foam@grephene and carbon paper@grephene with a solution of $Li_2C_2O_4$/DMSO wetting. The only characteristic peak derived from $Li_2C_2O_4$ at 290.4 eV has been detected on Ni foam@graphene cathode, while the peak at 289.6 eV is associated with Li_2CO_3 are present on carbon paper@graphene cathode, indicating the stabilizing effect of Ni foam on $Li_2C_2O_4$.

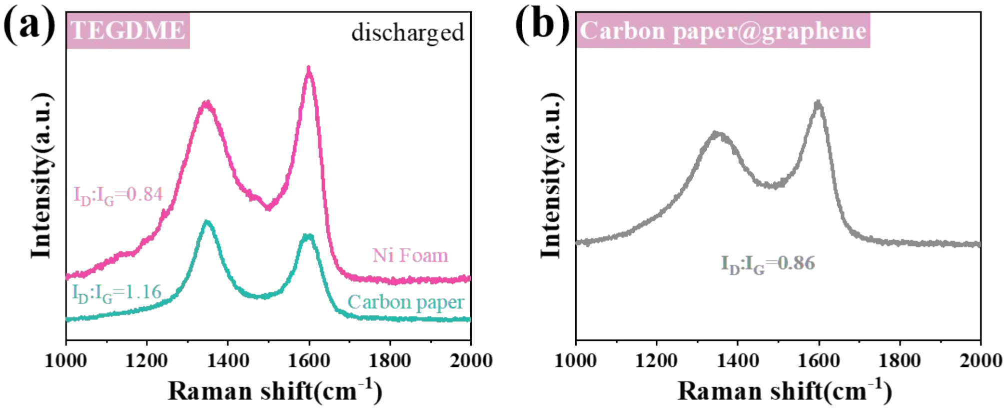

Figure S16. Raman spectra of (a) graphene@carbon paper and graphene@Ni foam cathode after discharge at 200 mA/g and (b) pristine carbon paper@graphene.

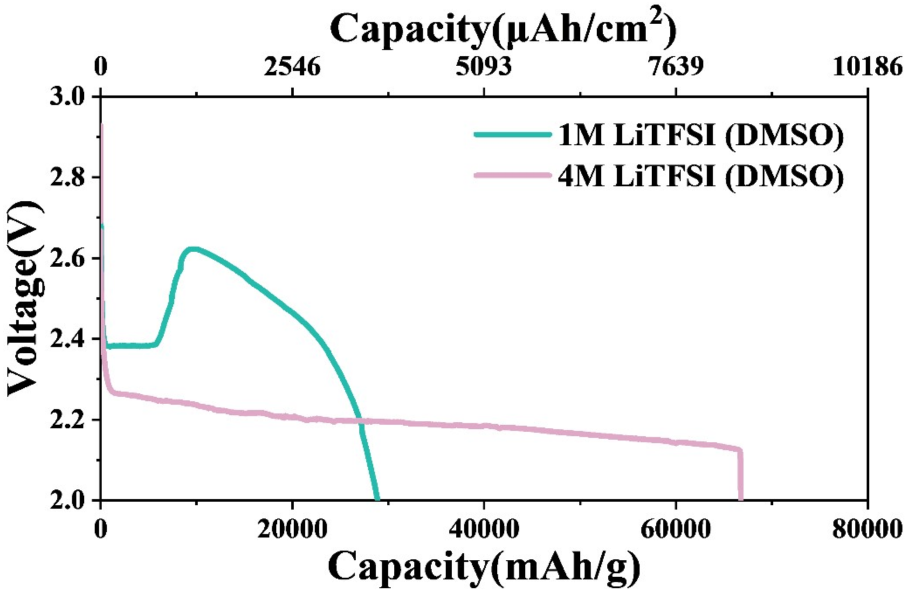

Figure S17. The voltage–capacity profiles of Li-CO_2 battery using different electrolytes discharged to 2.0 V at 200 mA g^{-1}. Li-CO_2 battery using 4 M LiTFSI (DMSO) as electrolyte shows a capacity of 66763 mAh/g, it's 2.3 times more than 1 M LiTFSI (DMSO) (28878 mAh/g).

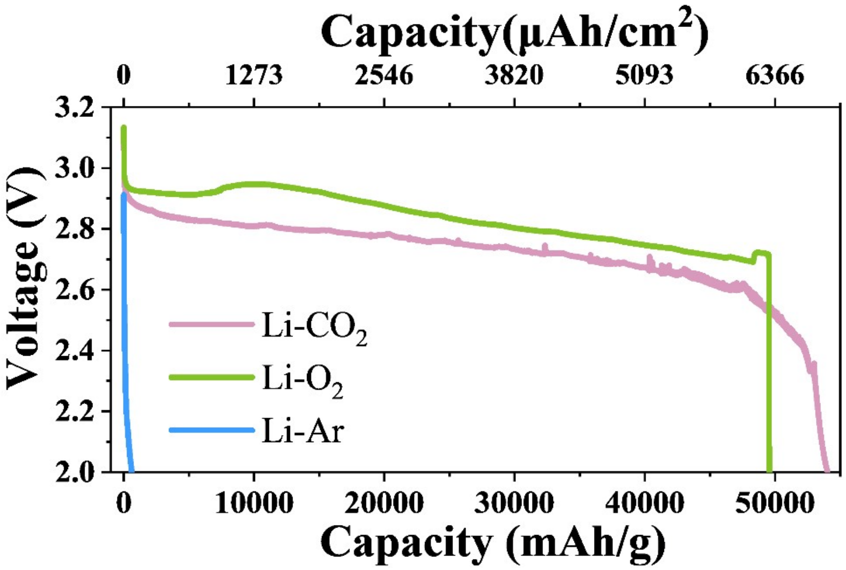

Figure S18. The voltage-capacity profiles of Li-CO_2, Li-O_2 and Li-Ar battery using 4 M LiTFSI (DMSO) as electrolyte at 200 mA/g with a cutoff potential of 2 V.

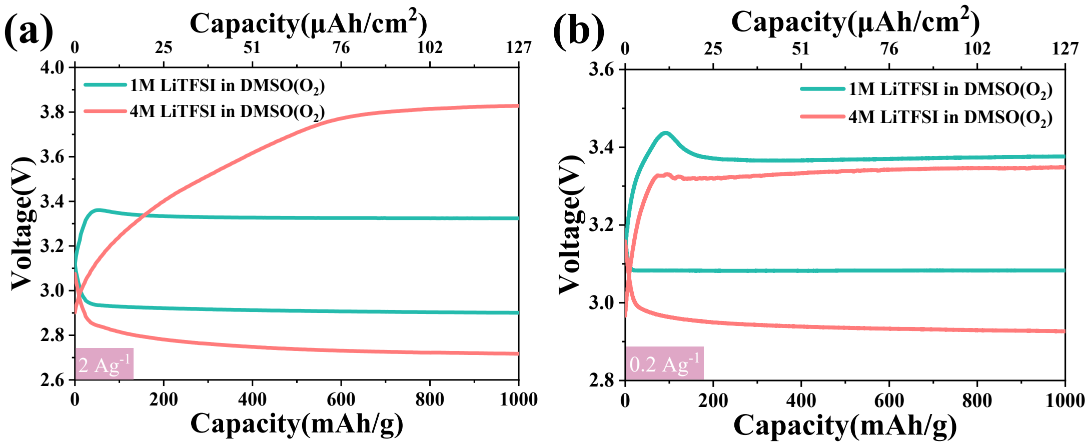

Figure S19. The discharge-charge curves of the Li-O_2 battery using the same condition with the Li-CO_2 battery at different current density a) 2 A/g and b) 0.2 A/g.

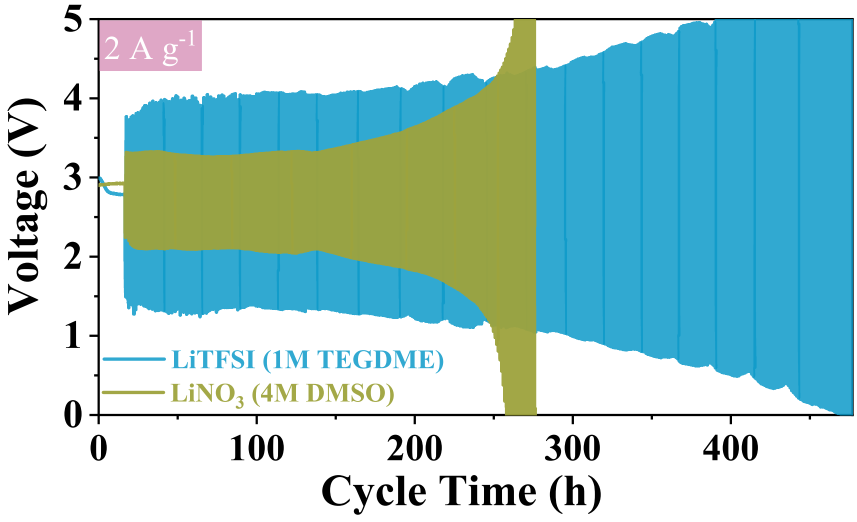

Figure S20. The discharge–charge profiles at 2 A/g in 1M LiTFSI (TEGDME) and 4M $LiNO_3$ (DMSO) with PTFE cover accompanied a cutoff capacity of 1000 mAh/g.

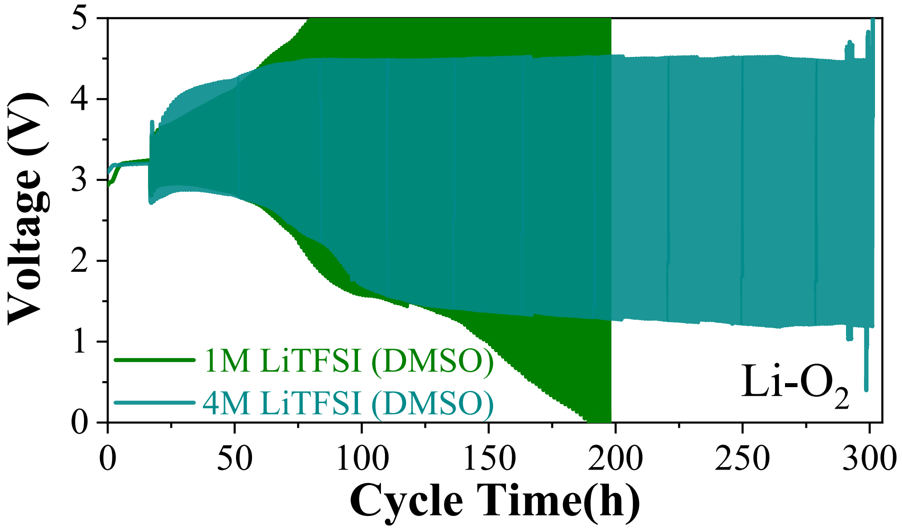

Figure S21. The discharge–charge profiles of Li-O_2 battery at 2 A/g in 1M and 4M LiTFSI (DMSO) with PTFE cover with cutoff capacity of 1000 mAh/g.

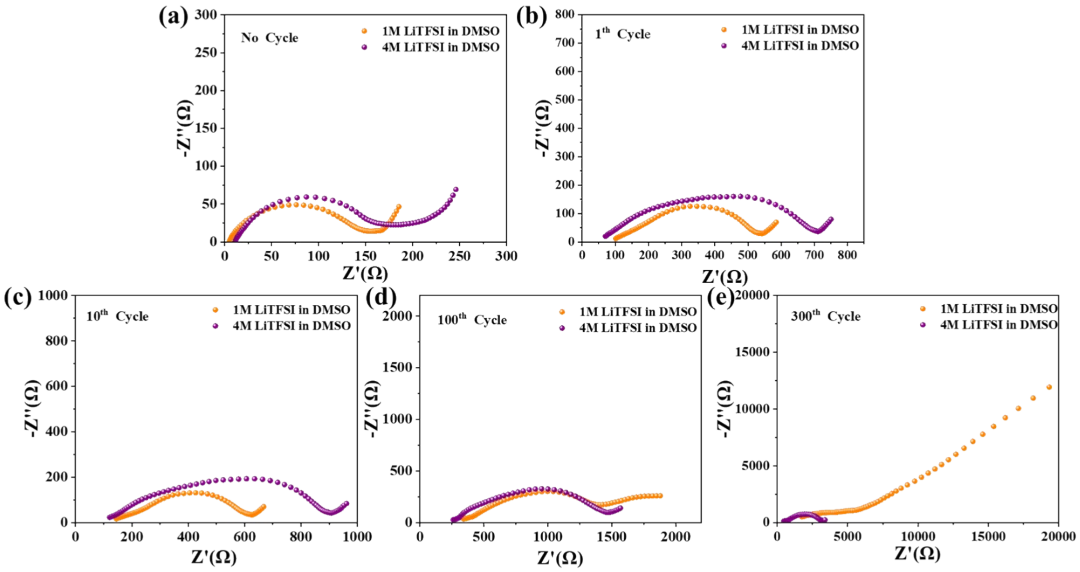

Figure S22. Electrochemical impedance spectra (EIS) of Li-CO_2 battery using different electrolytes (1 M LiTFSI (DMSO) and 4 M LiTFSI (DMSO)) after different cycles at the current density of 2 A/g.

Table S1. The binding energy (ΔE) of different solvation structures based on DFT calculation, the definition of ΔE indicates that a more negative value depicts a more stable solvation structure.

Solvent ΔE(Hartree) Structure	DMSO	GBL	PC	TEGDME
Li^+ + 1sol	-24.40264	-1.0054408	-20.7655382	-46.2914852
Li^+ + 2sol	-47.8466957	-1.0307665	-40.5566941	-91.3056738
Li^+ + 3sol	-71.2854858	-1.0402282	-60.3456072	—
Li^+ + 4sol	-94.706609	-1.0396458	-46.120173	—
Li^+ + $TFSI^-$ + 1sol	-0.0547881	18.0797344	-0.0623997	-0.1088254
Li^+ + $TFSI^-$ + 2sol	-0.0827754	36.1904879	-0.0890921	—
Li^+ + $TFSI^-$ + 3sol	-0.0800121	54.3202233	-0.1170226	—

Table S2. Comparison and summary of recent literatures on electrochemical performance of Li-CO_2 batteries.

Year	Electrolyte	Current density	Cut-off discharge/charge voltage	Cut-off capacity	Cycle performance	Ref.
2022	4 M LiTFSI/DMSO	2 A/g 4 A/g	2.0 V/3.2 V 1.65 V/3.4 V	1000 mAh/g	600 cycles	This work
2017	1 M LiTFSI/ TEGDME	1 A/g	2.75 V/4.25 V	1000 mAh/g	**200 cycles**	S1
2017	Bi-CoPc-GPE	0.1 A/g	~2.4 V/3.4 V	1000 mAh/g	100 cycles	S2
2018	1 M LiTFSI/ TEGDME	0.5 A/g	2.75 V/4.0 V	1000 mAh/g	**400 cycles**	S3
2018	0.3 M $LiNO_3$/1 M LiTFSI/DMSO	1 A/g	~2.6 V/4.25 V	500 mAh/g	235 cycles	S4
2018	1 M LiTFSI/ TEGDME	0.05 A/g	~2.7 V/4.25 V	1000 mAh/g	42 cycles	S5
2018	1 M LiTFSI/ TEGDME	0.2 A/g	~2.8 V/3.8 V	1000 mAh/g	50 cycles	S6
2019	0.1 M LiTFSI in (EMIM-BF_4)/DMSO	0.5 A/g	~2.8 V/4.2 V	500 mAh/g	**500 cycles**	S7
2019	1 M LiTFSI/ TEGDME	1 A/g	2.5 V/3.5 V	1000 mAh/g	360 cycles	S8

2019	1 MLiClO$_4$/ TEGDME	1 A/g	~2.5 V/4.0 V	1000 mAh/g	378 cycles	S9
2019	1 M LiTFSI/ TEGDME	0.4 A/g	~2.6 V/4.15 V	1000 mAh/g	190 cycles	S10
2020	Gel–polymer electrolyte	0.2 A/g	2.6 V/4.3 V	500 mAh/g	**538 cycles**	S11
2020	1 M LiTFSI/ TEGDME	0.1 A/g	~2.4 V/4.0 V	400 mAh/g	316 cycles	S12
2020	1 M LiTFSI/ TEGDME	0.1 A/g	2.5 V/4.25 V	500 mAh/g	200 cycles	S13
2021	1 M LiTFSI/ TEGDME	0.1 A/g	2.75 V/4.18 V	500 mAh/g	148 cycles	S14
2021	1M LiCF$_3$SO$_3$/ TEGDME	0.1 A/g	~2.5 V/4.1 V	1000 mAh/g	159 cycles	S15
2021	0.3 M LiNO$_3$/1 M LiTFSI/DMSO	1 A/g	~2.65 V/4.3 V	500 mAh/g	**600 cycles**	S16

References:

S1. L. Qie, Y. Lin, J. W. Connell, J. Xu and L. Dai, *Angew. Chem. Int. Ed.*, 2017, 56, 6970-6974.

S2. X. Hu, Z. Li and J. Chen, *Angew. Chem. Int. Ed.*, 2017, 56, 5785-5789.

S3. Y. Xing, Y. Yang, D. Li, M. Luo, N. Chen, Y. Ye, J. Qian, L. Li, D. Yang and F. Wu, *Adv. Mater.* , 2018, 30, 1803124.

S4. Y. Jin, C. Hu, Q. Dai, Y. Xiao, Y. Lin, J. W. Connell, F. Chen and L. Dai, *Adv. Funct. Mater.*, 2018, **28**, 1804630.

S5. X. Zhang, C. Wang, H. Li, X. Wang, Y. Chen, Z. Xie and Z. Zhou, *J. Mater. Chem. A*, 2018, 6, 2792-2796.

S6. Z. Zhang, Z. Zhang, P. Liu, Y. Xie, K. Cao and Z. Zhou, *J. Mater. Chem. A*, 2018, 6, 3218-3223.

S7. A. Ahmadiparidari, R. E. Warburton, L. Majidi, M. Asadi, A. Chamaani, J. R. Jokisaari, S. Rastegar, Z. Hemmat, B. Sayahpour and R. S. Assary, *Adv. Mater.*, 2019, 31, 1902518.

S8. X. Li, J. Zhou, J. Zhang, M. Li, X. Bi, T. Liu, T. He, J. Cheng, F. Zhang and Y. Li, *Adv. Mater.*, 2019, 31, 1903852.

S9. Y. Mao, C. Tang, Z. Tang, J. Xie, Z. Chen, J. Tu, G. Cao and X. Zhao, *Energy Stor. Mater.*, 2019, **1**8, 405-413.

S10. H. Wang, K. Xie, Y. You, Q. Hou, K. Zhang, N. Li, W. Yu, K. P. Loh, C. Shen and B. Wei, *Adv. Energy Mater.*, 2019, 9, 1901806.

S11. L. Song, C. Hu, Y. Xiao, J. He, Y. Lin, J. W. Connell and L. Dai, *Nano Energy*, 2020, 71, 104595.

S12. G. Wu, X. Li, Z. Zhang, P. Dong, M. Xu, H. Peng, X. Zeng, Y. Zhang and S. Liao, *J. Mater. Chem. A*, 2020, 8, 3763-3770.

S13. S. Thoka, C. Chen, A. Jena, F. Wang, X. Wang, H. Chang, S. Hu and R. Liu, *ACS Appl. Mater. Interfaces*, 2020, 12, 17353-17363.

S14. C. Chen, C. Huang, Y. Huang, F. Wang, X. Wang, C. Wu, W. Chang, C. Dong, L. Yin and R. Liu, *ACS Appl. Mater. Interfaces*, 2021, 13, 6156-6167.

S15. C. Wang, Y. Lu, S. Lu, S. Ma, X. Zhu, Z. Li and Q. Liu, *J. Power Sources*, 2021, 495, 229782.

S16. F. Ye, L. Gong, Y. Long, S. N. Talapaneni, L. Zhang, Y. Xiao, D. Liu, C. Hu and L. Dai, *Adv. Energy Mater.*, 2021, 11, 2101390.